Tellus (2002), 54B, 213–230
Printed in UK. All rights reserved

Copyright © Munksgaard, 2002
TELLUS
ISSN 0280–6509

A pseudo-Lagrangian study of the sulfur budget in the remote Arctic marine boundary layer

By E. DOUGLAS NILSSON* and CAROLINE LECK, *Department of Meteorology, Stockholm University, S-106 91 Stockholm, Sweden*

(Manuscript received 21 September 2000; in final form 2 December 2001)

ABSTRACT

The atmospheric sulfur cycle of the remote Arctic marine boundary layer is studied using trajectories and measurements of sulfur compounds from the International Arctic Ocean Expedition 1991, along with a pseudo-Lagrangian approach and an analytical model. The dimethyl sulfide [DMS(g)] turnover time was 59^{+18}_{-9} h. Only 25^{+11}_{-9}% of DMS(g) followed reaction paths to sulfur dioxide [SO_2(g)], sub-micrometre aerosol non-seasalt sulfate (nss-SO_4^{2-}) or methane sulfonate (MSA). During the first 3 d of transport over the pack ice, fog deposition and drizzle resulted in short turnover times; 16^{+8}_{-6} h for SO_2(g), 18^{+4}_{-4} h for MSA and 18^{+2}_{-3} h for nss-SO_4^{2-}. Therefore, DMS(g) will, owing to its origin along or south of the ice edge and longer turnover time, survive the original sub-micrometre sulfur aerosol mass and gradually replace it with new biogenic sulfur aerosol mass. The advection of DMS(g) along with heat and moisture will influence the clouds and fogs over the Arctic pack ice through the formation of cloud condensation nuclei (CCN). If the pack ice cover were to decrease owing to a climate change, the total Arctic Ocean DMS production would change, and potentially there could be an ice–DMS–cloud–albedo climate feedback effect, but it would be accompanied by changes in the fog aerosol sink.

1. Introduction

The hypothesis of Charlson et al. (1987) postulates that biogenic dimethyl sulfide (DMS) production by marine phytoplankton can exert a climate control. The hypothesis states that DMS is transferred from the ocean to the atmosphere and oxidized to form sulfur particles. Some of these grow large enough to act as cloud condensation nuclei (CCN), which regulate the number of cloud droplets and thus indirectly the cloud reflectivity (Tomey, 1974). For a verification of the postulated DMS–CCN–cloud–climate feedback, the two most important processes to study would be the sensitivity to temperature of new particle formation and early growth and DMS production and oxidation. Such processes would be most effective in oceanic regions away from sources of anthropogenic sulfur gases.

The central Arctic Ocean in summer and early autumn fulfills the remote requirement as it experiences a freedom from continental and anthropogenic sources. The air tends to either be imported from the North Atlantic Ocean or to circulate over the Arctic Ocean basin (Nilsson, 1996; Nilsson and Barr, 2001). Cloudiness also has an annual maximum, with optically thin stratus layers predominating (e.g. Curry, 1995), which constitutes an added advantage for testing aerosol–cloud property relationships. The International Arctic Ocean Expedition in the summer and autumn of 1991 (IAOE-91) (Leck et al., 1996; and other papers within the same special issue of *Tellus B*) demonstrated that over the pack ice area, local contribution to the atmospheric DMS

* Corresponding author.
e-mail: dolan@misu.su.se

concentrations can be assumed to be negligible compared to that advected from the marine source south along the ice edge (Leck and Persson, 1996a,b). The production of CCN by condensation of DMS oxidation products on sub-CCN particles, being advected over the pack ice, should thus be very important in controlling the available sulfur and could consequently be important for cloud formation over the ice-covered Arctic Ocean.

The atmospheric biogenic sulfur life cycle involves several steps: (1) gas-phase oxidation of DMS (in daytime with the OH radical, at night with the NO_3 radical), (2) gas-to-particle transformation of its oxidation products, and (3) removal of these products from the atmosphere by dry and wet deposition. The chemical and physical pathways which lead from atmospheric DMS(g) to sulfur particles are very complex and still poorly understood. The two most important end products from DMS(g) oxidation, particulate non-sea-salt sulfate (nss-SO_4^{2-}) and methane sulfonate (MSA), evolves via the formation of the gases sulfur dioxide [SO_2(g)], sulfuric acid [H_2SO_4(g)] and methaneesulfonic acid [MSA(g)] (Yin et al., 1990a,b; Capaldo and Pandis, 1997; Campolongo et al., 1999; Davis et al., 1999; Koga and Tanaka, 1999). Observations also suggest a pathway over SO_3 to H_2SO_4(g) (Bandy et al., 1992; Lin and Chamides, 1993). Additional oxidation products (Hynes, 1996) are dimethyl sulfoxide (DMSO) and dimethyl sulfone ($DMSO_2$). In the liquid phase, SO_2(aq) can react with hydrogen peroxide (H_2O_2) or ozone (O_3) to form sulfate (Chamides and Stelsson, 1992).

The purpose of this study is to gain further knowledge on the biogenic sulfur budget in the remote marine boundary layer over the central Arctic Ocean. To do that we will make use of ice maps, trajectories, and chemical and meteorological data from the IAOE-91 and of an analytical model.

2. Experimental approach

2.1. The study area

The measurements to be discussed were performed on board the Swedish icebreaker *Oden* between 1 August and 6 October 1991. The expedition covered sampling between 75°N and 90°N in the open waters and along the ice edge zone in the Greenland Sea — Fram Strait area, as well as in the permanent pack ice of the Nansen, Amundsen and Makarov basins (Fig. 1). Atmospheric measurements were mainly made on 13 separate 24 h sampling stations.

The ice cover was on average 90% during August and early September (summer) with many leads (openings between ice floes) even at the North Pole, and the ice floes were partly covered with melt ponds, see Leck and Persson (1996a) and Liljeström (1992). After mid-September (autumn) all open leads and ponds began to freeze. In Fig. 1 we have illustrated the geographical distribution of the location of the ice edge during IAOE-91. During the expedition the sun was continuously above the horizon until 13 September.

2.2. Experimental methods

A size-segregating inlet (<1 μm diameter) for simultaneous sampling of atmospheric aerosols and gases was used. Contamination from the ship was excluded by a condensation nuclei control with a wind sector controller; see Leck et al. (1996) for more details.

2.2.1. Atmospheric radon and DMS. The concentration of radon (Rn) was estimated from alpha-emitting radon daughters captured on a filter and logged every minute, see Bigg (1996). Atmospheric DMS concentrations were obtained from a system using gas chromatography with flame photometric detection, see Persson and Leck (1994), and preconcentration for up to 60 min [flow $\sim$1 standard litre per min (slmp)] in a cold trap (liquid argon). Oxidants were scavenged using a cotton scrubber and a Nafion drier. The detection limit for the method was 1 ppt(v), and the overall accuracy of the analysis was within $\pm$12%.

2.2.2. Atmospheric aerosol particles and sulfur dioxide. Concentrations of particulate mass of MSA and nss-SO_4^{2-} and gas-phase SO_2 were determined using two ambient parallel filter pack (FP) sets for the aerosol (flow rate 90 slpm) and one FP set for SO_2 (flow rate 45 slpm). In each of the sets, two units collected samples and one served as a sampling and an analytical blank. Collection times ranged from 4 to 24 h. The ionic mass of the major cations and anions and MSA was determined by chemically suppressed ion

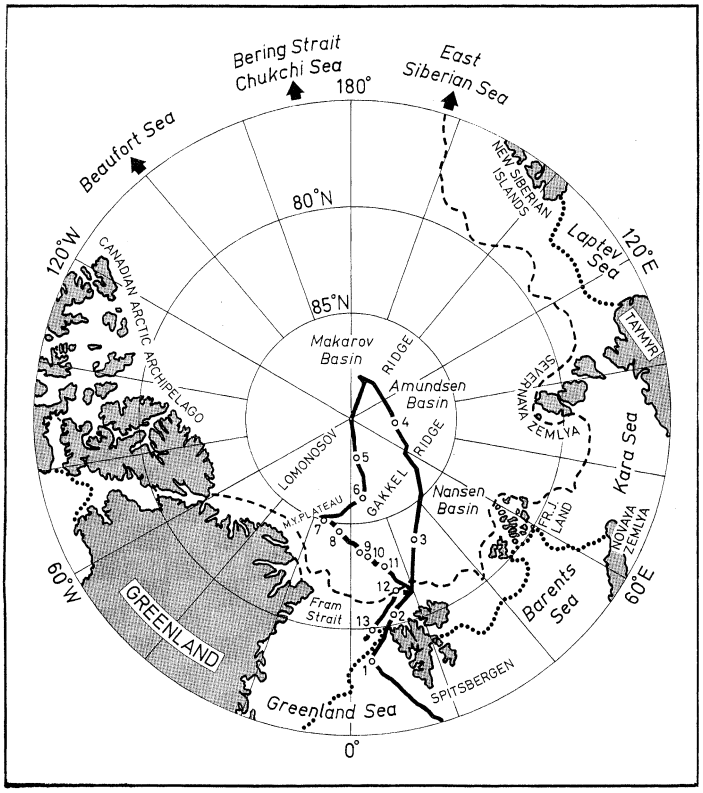

Fig. 1. Map of the Arctic Ocean with maximum (dotted line) and minima (dashed line) ice cover between 1 August and 6 October (Julian days 212–279) 1991 and the cruise track (thick line) of the ice breaker *Oden*. Reproduced from Leck et al. (1996).

chromatography. The analysis should show mainly sub-micrometre mass, since a cyclone on the sampling line was used to remove particles larger than ~ 1 μm diameter. More details are given by Leck and Persson (1996b).

Each pair of duplicate samples was individually blank corrected. Nss-SO_4^{2-} concentrations were calculated from sodium concentrations and seawater composition (Stumm and Morgan, 1981). The sea-salt contribution was on average less than 4% of the total sub-micrometre SO_4^{2-}. The average particulate MSA, nss-SO_4^{2-} and gas-phase SO_2 blank concentrations were $<3\%$, 5% and 40% of the sample, respectively. Duplicate samples (quadruplicate for the FP) for all particulates agreed on average within 15%. Levels (sample minus blank) of SO_2, MSA, and nss-SO_4^{2-} down to 0.05, 0.002 and 0.03 nmol m^{-3} were detected. All atmospheric gas and particulate phase data are expressed in mass per m^3 at standard temperature and pressure (STP; 273.15 K and 1013.2 hPa), such that 1 nmol $m^{-3} = 22.4$ ppt(v).

2.2.3. Meteorological data. Hourly or half-hourly meteorological observations of wind speed and direction, air temperature, pressure, relative humidity (RH), visibility, cloud cover, precipitation and cloud type (including fogs) were made. Rawinsonde, released at intervals of the order of 6 h, recorded vertical distribution of RH, temperature, pressure, wind speed and direction. See Nilsson (1996) and Nilsson and Bigg (1996) for details. To follow changes in and extension of the pack ice, maps prepared by NESDIS/Synoptic Analysis Branch (based on NOAA-11 and GOES-7 images) and by the Norwegian Meteorological Institute (based on satellite and ship observations) have been used.

The history of each air sample was derived from 5–10 d three-dimensional backward trajectories, reaching the ship's position and pressure level at 0, 6, 12 and 18 UTC. The trajectories were calculated with the McGrath (1989) trajectory model, using the analyzed horizontal and vertical wind and mass fields of the European Centre for Medium Range Weather Forecasts (ECMWF, 1994: The description of the ECMWF/WCRP Level III-A Global Atmospheric Data Archive). Nilsson (1996) found that the model resolves surface and line sources >5 d backward and point or small surface sources 2–4 d in the Arctic.

3. An analytical pseudo-Lagrangian model

3.1. The pseudo-Lagrangian approach

An ideal way to achieve knowledge of sink and source rates for substances in the atmosphere is to sample in the same air volume as it is transported with the wind, a Lagrangian study (e.g. Johnson et al., 2000). The observed rates of change of concentrations is then the key information to understand the chemical processes and budget, but true Lagrangian measurements are logistically difficult to perform.

Gas-phase SO_2, and MSA and nss-SO_4^{2-} in the sub-micrometre aerosol, have both sources and sinks over the central Arctic Ocean, so steady-state assumptions might be useful, at least if sources and sinks are equal. North of the ice edge we are remote from the source of DMS, so steady-state assumptions cannot be used, and if the measurements are not Lagrangian, the observed rate of change will be largely influenced by advection. However, measurements made in different air parcels can be used for a Lagrangian approach if the source location is known. Transport times and distances from the source can be derived from backward trajectories and combined with measurements to calculate the sink rate and turnover time of the substance. We will call this a pseudo-Lagrangian method.

Since the pack ice of the central Arctic Ocean provided us with a lid on the ocean, which prevents DMS emissions, we can calculate the transport time and distance from open sea from trajectories and ice maps, hereafter referred to as the marine transport time (t_m), Fig. 2a. A second set of transport times, referred to as the crustal transport time (t_c), was derived from trajectories in combination with maps and information about snow cover and glaciers (not shown). Nilsson (1996) found t_m and t_c to be well correlated with DMS(g) and Rn concentrations, with open sea and land origins, respectively. Because of the marine origin of DMS, higher DMS(g) concentrations were observed when the air more recently had been over the open sea, and lower DMS(g) concentrations were observed when the air had spent a long time over the pack ice, cf. Figs. 2a and 2b. Similar behavior can partly be seen in Figs. 2c–e between t_m and the time evolution of the SO_2(g), and MSA and nss-SO_4^{2-} sulfur compounds.

Since radioactive decay is the only Rn sink, it can be used to validate the method. Using the best linear fit between the logarithm of the Rn concentration (c_{Rn}) and t_c (not shown), the rate of change is

$$\frac{dc_{Rn}}{dt_c} = -k_{Rn} c_{Rn} \quad (1)$$

The slope between the logarithm of c_{Rn} and t_c is $k_{Rn} = 2.1 \times 10^{-6}\ s^{-1}$ (the disintegration constant), and the half-life

$$\tau_{1/2Rn} = \frac{\ln 2}{k_{Rn}} \quad (2)$$

is 91 h, which is close to the true value (91.7 h), but of bad precision (46–170 h with 90% confidence interval). As we shall see, the correlation between t_m and DMS(g) was better than between t_c and Rn, and the confidence interval was narrower. This is probably because the land Rn sources were on average 2 d more distant than the ocean DMS sources and close to the limit where the trajectories becomes statistically unreliable. Furthermore, some Rn results from small islands within the Arctic which are hard for the trajectory model to resolve.

3.2. Data selection

While Figs. 2b–e include all available samples, it became obvious that some samples were not suitable for our study, e.g. if there was a large anthropogenic component in the aerosol or the air had not been over the open sea for a very long time. In order to select a data set useful for the pseudo-Lagrangian approach and representative of the MBL biogenic sulfur cycle the following

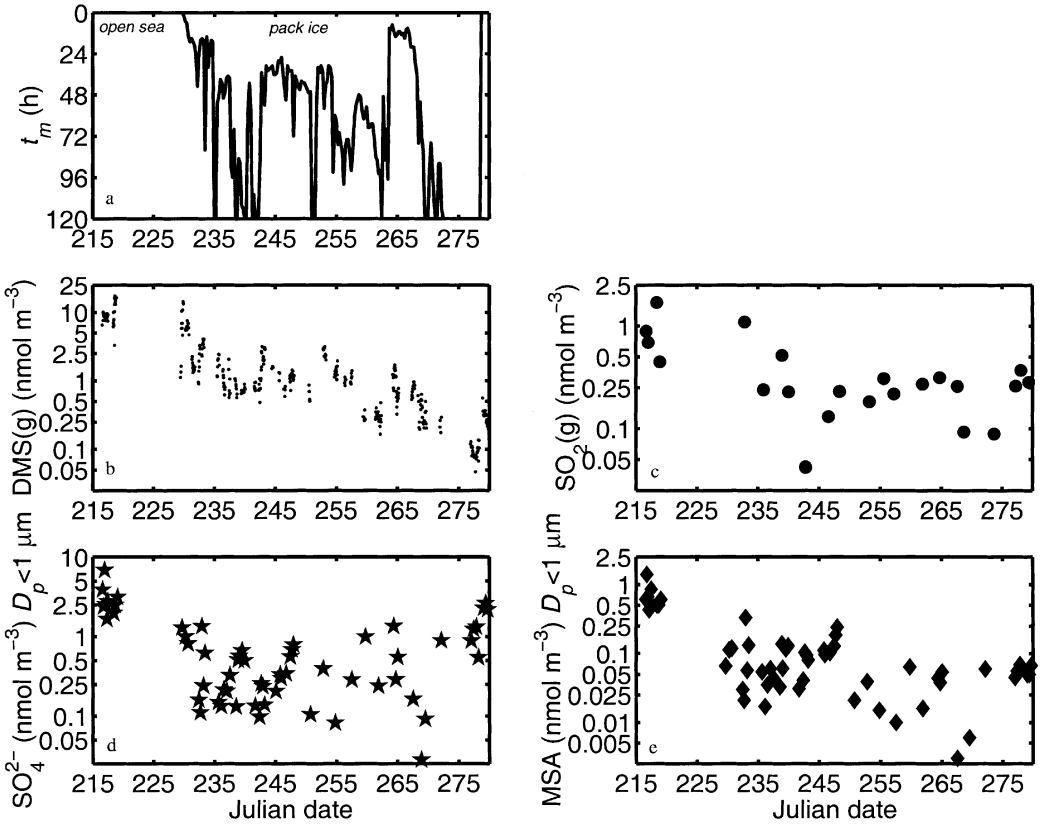

Fig. 2. (a) Marine transport time (t_m) during IAOE-91 as a function of Julian date. In open sea, $t_m = 0$. (b) Same as (a), but for the concentration of DMS(g). The figure includes all samples. (c) Same as (b), but for SO_2(g). (d) Same as (b), but for sub-micrometre nss-SO_4^{2-}. (e) Same as (b), but for sub-micrometre MSA.

sorting criteria were used: (1) Samples collected in air considerably influenced by anthropogenic sources were omitted from the data selection, using elevated concentrations of elemental carbon as a tracer for combustion sources (Leck and Persson, 1996b). (2) Samples taken in air that subsided from the free troposphere (FT) over the ice were excluded from the data set. This does not exclude air entrained from the FT on a smaller scale. (3) Also excluded were samples in air that spent too short a time over open sea for the sulfur system to approach equilibrium with the marine DMS source. (4) Leck and Persson (1996a) demonstrated that the marginal ice edge zone (MIZ) offered a local DMS source 50% less than or equal to the advected DMS(g), which can cause an overestimation of dc_{DMS}/dt_m. In summer this was the case for $t_m < 17$ h, which corresponds to the observed MIZ width, while in autumn the effect is less pronounced with a narrower MIZ and a weaker local source. Therefore, DMS(g) samples for $t_m < 17$ h have been omitted. (5) Most of the wide range of t_m includes samples from both summer and autumn. However, for $t_m \leqslant 4$ h and $t_m > 108$ h there are only DMS(g) samples from early in the expedition. These DMS(g) samples have been omitted. (6) Aerosol samples made in fog or snowfall during most of the sampling period are not included, since their mass comes mainly from the interstitial aerosol and since part of the activated fraction of the aerosol may return to the MSA and nss-SO_4^{2-} boxes of our system when the fog evaporates.

The remaining samples, about 80% of the total, covered the period Julian Day 216 (4 August) to 269 (26 September), see Fig. 3. An explanation of

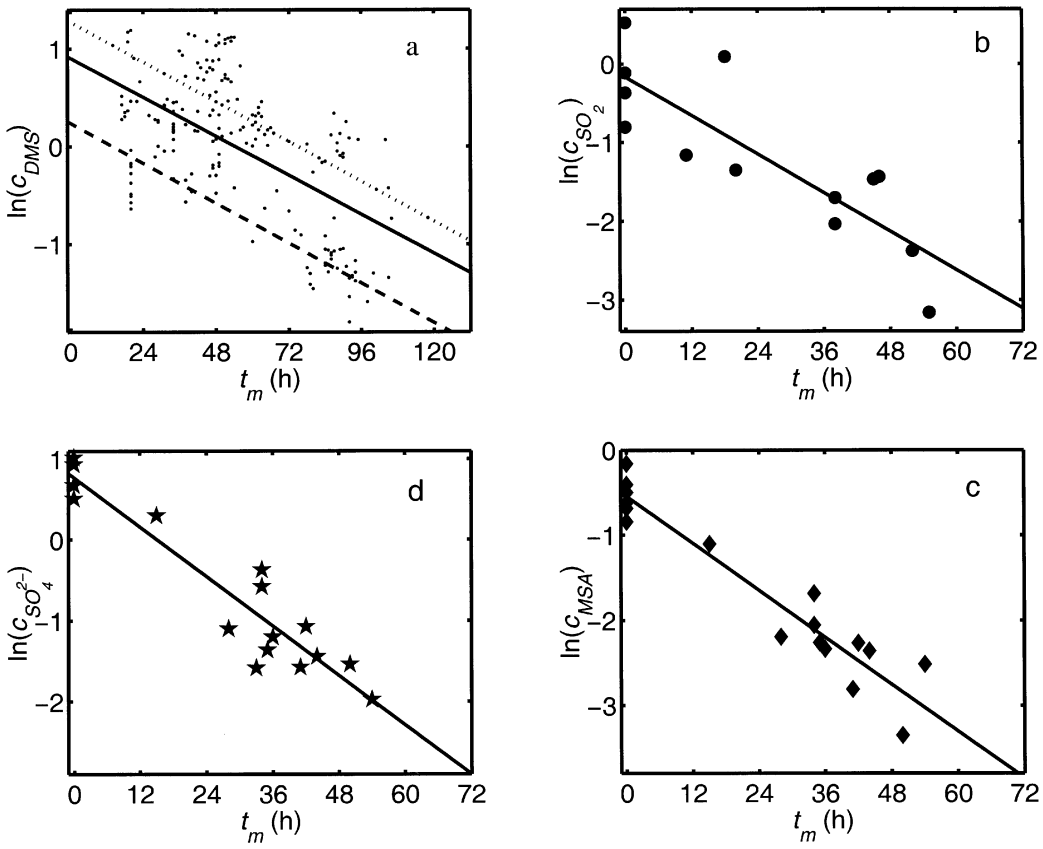

Fig. 3. (a) Logarithmic concentration of the selected DMS(g) samples against marine transport time (t_m), including the best linear fit (full line). Also shown are the best fits of the summer sub-set (dotted line) and the autumn sub-set (dashed line). (b) Same as (a), but for SO_2(g). The figure shows the best linear fit to the first three days of transport. (c) Same as (a), but for nss-SO_4^{2-}. The figure shows the best linear fit for the first three days. (d) Same as (a), but for MSA. The figure shows the best linear fit for the first three days.

the linear fits in Fig. 3 and the uncertainty analysis will follow in Section 4. The selections are more representative of the summer (ending around mid-September with the freeze-up) than the autumn, and are valid for the initially cloudy and foggy conditions when relatively warm marine air is advected in over the pack ice and aged there to a colder and less cloudy air.

3.3. *The system of equations*

From the source, reaction and sink pathways outlined in the introduction for the natural biogenic sulfur system, we can write the rates of change of concentrations with t_m as:

$$\frac{dc_{DMS}}{dt_m} = Q_{DMS} - S_{DMS} - k_{DMS\rightarrow SO_2} c_{DMS} - k_{DMS\rightarrow MSA} c_{DMS} - k_{DMS\rightarrow nss\text{-}SO_4^{2-}} c_{DMS} - k_{DMS\rightarrow ?} c_{DMS} \quad (3a)$$

$$\frac{dc_{SO_2}}{dt_m} = Q_{SO_2} - S_{SO_2} + k_{DMS\rightarrow SO_2} c_{DMS} - k_{SO_2\rightarrow nss\text{-}SO_4^{2-}} c_{SO_2} - k_{dep\text{-}SO_2} c_{SO_2} \quad (3b)$$

$$\frac{dc_{MSA}}{dt_m} = Q_{MSA} - S_{MSA} + K_{DMS\rightarrow MSA}c_{DMS} - k_{dep\text{-}MSA}c_{MSA} \quad (3c)$$

$$\frac{dc_{nss\text{-}SO_4^{2-}}}{dt_m} = Q_{nss\text{-}SO_4^{2-}} - S_{nss\text{-}SO_4^{2-}} + k_{DMS\rightarrow nss\text{-}SO_4^{2-}}c_{DMS} + k_{SO_2\rightarrow nss\text{-}SO_4^{2-}}c_{SO_2} - K_{dep\text{-}nss\text{-}SO_4^{2-}}c_{nss\text{-}SO_4^{2-}} \quad (3d)$$

where each c, Q or S is a concentration, source or sink, respectively. Each k is the sum of the products of reaction rates and the concentration of the oxidant for all reaction paths from each substance to a product.

Included is a path representing an unknown DMS sink out of the system to a box not measured. This sink refers e.g. to the proposed OH addition pathway to DMSO and $DMSO_2$ or to the aqueous phase reaction of DMS with O_3 in droplets as suggested by Lee and Zhou (1994). Effects of horizontal divergence and diffusion have not been included and are believed to be small due to the limited turbulent diffusion in the Arctic MBL and the line or area source nature of DMS emissions. Marine air should generally invade the pack ice with small horizontal concentration gradients perpendicular to the wind direction. There may be a significant sink or source effect of vertical mixing and entrainment/detrainment between the MBL and the FT, which we will include in, respectively, Q or S. However, the vertical turbulent diffusion is generally small owing to the high static stability of the boundary layer and lower troposphere over the pack ice (Nilsson, 1996; Paluch et al., 1997; Nilsson et al., 2001). Q_{DMS} also includes the flux of DMS from the sea. As pointed out in the introduction, over the pack ice the flux of DMS is greatly reduced because of the ice cover. It is therefore set to zero, except in the MIZ, where we have examined the influence of a local source. Each deposition rate k represents the sum of dry as well as wet deposition. We assume that DMS deposition to sea and ice is negligible (Lee and Zhou, 1994).

3.4. *Approximations*

To make the system of four equations (3a)–(3d) solvable we will have to approximate values of the rates of change on the left side of the equations, and replace four of the eight unknowns on the right side of the equations with approximations. If the left side of eqs. (3a)–(3d) equal zero we can derive a steady-state solution, but this is not applicable over the central Arctic Ocean pack ice. However, the rates of change can be replaced by empirically estimated values.

If we neglect Q_{DMS} and S_{DMS} over the pack ice and introduce a constant k_{DMS}, the sum of all oxidation rates of DMS(g), we can rewrite eq. (3a) as

$$\frac{dc_{DMS}}{dt_m} = -k_{DMS}c_{DMS} \quad (4)$$

If k_{DMS} is a constant, c_{DMS} should decline exponentially with time. If we plot the logarithmic concentration against t_m (Fig. 3), then k_{DMS} is the slope:

$$k_{DMS} = -\frac{\ln\left(\frac{c_{DMS}(t_m)}{c_{DMS}(0)}\right)}{t_m}, \quad (5)$$

and the turnover time of DMS(g) can be calculated according to

$$\tau_{0\text{-}DMS} = \frac{1}{k_{DMS}}. \quad (6)$$

This timescale may also be referred to as the 'e-folding time' or the 'response time' characterizing the decay in concentration during the transport in over the pack ice. For simple linear models, like ours, it is identical to the turnover time. The rate of change of c_{DMS} with t_m expressed in eq. (4) can be calculated from the estimated k_{DMS} to replace the left side of eq. (3a).

For SO_2(g), MSA and nss-SO_4^{2-} there are many fewer data points, since the sampling time was so much longer than for DMS. The evolution of SO_2(g), MSA and nss-SO_4^{2-} will not follow a simple exponential decline, since they have both sources and sinks over the pack ice. Only if they are in steady state can the left side of eqs. (3b)–(3d) be replaced with zero. However, if we can make a quantitative estimate of the rates of change it will be possible to replace the left side of eqs. (3b)–(3d) with a value other than zero. It is reasonable to find a close to exponential decline in SO_2(g), MSA and nss-SO_4^{2-} concentrations if their sources are smaller than their sinks. The good log-linear fits in Figs. 3b–d suggest that this was the case for SO_2(g), MSA and nss-SO_4^{2-} for $t_m \leqslant 3$ d (see

Table 1 for statistics). For $t_m > 3$ d there was no significant trend in SO_2(g), MSA or nss-SO_4^{2-}, but the average concentrations are given in Table 1.

We can now estimate

$$\frac{dc_{SO_2}}{dt_m} \approx -k_{SO_2} c_{SO_2}, \quad \frac{dc_{MSA}}{dt_m} \approx -k_{MSA} c_{MSA},$$

$$\frac{dc_{SO_4^{2-}}}{dt_m} \approx -k_{SO_4^{2-}} c_{SO_4^{2-}} \qquad (7a\text{–}c)$$

where k_{SO_2}, k_{MSA} and $k_{SO_4^{2-}}$ are the respective best-fit slopes. Without sources k_{SO_2}, k_{MSA} and $k_{SO_4^{2-}}$ would be the total sink rates, but they are now instead lower limits. Their inverse values are upper limits for their average turnover times.

On the right side of the system of four equations (3a)–(3d) we will use the following four approximations:

$$k_{DMS \to MSA} = \alpha k_{DMS \to SO_2} \qquad (8a)$$

$$k_{DMS \to nss\text{-}SO_4^{2-}} = 0 \qquad (8b)$$

$$k_{DMS \to ?} = \beta(1 + \alpha) k_{DMS \to SO_2} \qquad (8c)$$

$$k_{dep\ sub\text{-}\mu m} = k_{dep\text{-}MSA} = k_{dep\text{-}nss\text{-}SO_4^{2-}} \qquad (8d)$$

where α is the a branching factor between the two reaction pathways for DMS(g) to SO_2(g) and MSA, assuming $\alpha = 0.22$ (Leck and Persson, 1996b), the average molar ratio between the sub-micrometre aerosol MSA and nss-SO_4^{2-} mass, and that most nss-SO_4^{2-} is formed via SO_2(g) and not SO_3 (Lin and Chamides, 1993), neglecting the hypothetical reaction path directly from DMS(g) to nss-SO_4^{2-}. We introduce a branching β between the unknown path of DMS(g) out of the system and the reaction paths to SO_2(g) and MSA. Finally, the deposition rate $k_{dep\ sub\text{-}\mu m}$ can be assumed to be identical for sub-micrometre aerosol MSA and nss-SO_4^{2-}, motivated by their similar mass size distributions (Bergin et al., 1995a; Leck and Persson, 1996b). Although this will allow us to solve the system of equations (3) we will have to test the solution for different β (see Section 4.3.1).

4. Results

4.1. Results derived from the rates of change of sulfur concentrations over the pack ice

4.1.1. Gas phase DMS. The general decreasing trend in DMS(g) concentration with t_m is evident

Table 1. *The best linear fits between the logarithmic concentration and the marine transport time*

	k (s^{-1})	σ (s^{-1})	95% (s^{-1})	r	p
			DMS(g)		
all, 17–108 h	-4.7×10^{-6}	5.6×10^{-7}	$(-5.6$ to $-3.6) \times 10^{-6}$	-0.570	$\leqslant 0.0001$
summer	-4.2×10^{-6}	5.6×10^{-7}	$(-5.0$ to $-3.3) \times 10^{-6}$	-0.723	$\leqslant 0.0001$
autumn	-4.7×10^{-6}	5.6×10^{-7}	$(-5.6$ to $-3.9) \times 10^{-6}$	-0.869	$\leqslant 0.0001$
compensated for z_{box}	-4.7×10^{-6}	1.4×10^{-6}	$(-7.5$ to $-2.2) \times 10^{-6}$	-0.591	0.0006
			SO_2(g)		
all, 0–72 h	-1.1×10^{-5}	2.2×10^{-6}	$(-1.6$ to $-0.7) \times 10^{-5}$	-0.847	0.0003
>72 h[a)]					
			MSA		
all, 0–72 h	-1.3×10^{-5}	1.1×10^{-6}	$(-1.5$ to $-1.1) \times 10^{-5}$	-0.953	$\leqslant 0.0001$
summer, 0–72 h	-1.3×10^{-5}	8.3×10^{-7}	$(-1.5$ to $-1.1) \times 10^{-5}$	-0.962	$\leqslant 0.0001$
>72 h[b)]					
			nss-SO_4^{2-}		
all, 0–72 h	-1.4×10^{-5}	1.4×10^{-6}	$(-1.7$ to $-1.1) \times 10^{-5}$	-0.942	$\leqslant 0.0001$
summer, 0–72 h	-1.4×10^{-5}	8.3×10^{-7}	$(-1.6$ to $-1.3) \times 10^{-5}$	-0.981	$\leqslant 0.0001$
>72 h[c)]					

Slopes of the best linear fits in Fig. 3 and uncertainty of the slopes: the standard deviation (σ), the 95% confidence interval, the correlation coefficient (r), and the probability that the correlation would occur by chance (p).

[a)] No significant fit was found. The mean concentration (m) and the standard deviation of the concentration (σ) were $m \pm \sigma = 0.256 \pm 0.041$.

[b)] No significant fit was found. $m \pm \sigma = 0.069 \pm 0.044$.

[c)] No significant fit was found. $m \pm \sigma = 0.352 \pm 0.258$.

in Fig. 3a. The scatter must be due to seasonal changes in source strength and photochemical reactions, geographical differences in source strength, and variations in MBL stability and depth (Leck and Persson, 1996a,b). The best log-linear fit in Fig. 3a has a slope $k_{DMS} = 4.7 \times 10^{-6}\,s^{-1}$, which is the total DMS(g) sink rate, and the corresponding average $\tau_{0\text{-}DMS} = 59$ h. The precision of this fit is much better than it was for Rn, for reasons already listed. The rate of change of c_{DMS} with t_m expressed in eq. (4) can now be calculated from the estimated k_{DMS} to replace the left side of eq. (3a). Before doing so we will investigate possible biases of the derived value of k_{DMS}.

The influence of the season can be examined by using DMS(g) samples from two shorter periods well separated in time, assuming that within each period there were small differences in DMS source strength and limited changes in photochemistry, while between them there should have been considerable changes. Two periods, one during the summer (Julian day 229–243) and one during the autumn (Julian day 264–269), had a wide enough variety in t_m owing to relatively rapid changes in weather pattern caused by cyclones entering the central Arctic Ocean. The best fit slopes of $3.9 \times 10^{-6}\,s^{-1}$ and $4.7 \times 10^{-6}\,s^{-1}$ for summer and autumn, respectively (Fig. 3a) correspond to $\tau_{0\text{-}DMS} = 71$ and 59 h. They are not significantly different from the overall fit or each other, which indicates that the seasonal trend in DMS sinks is small.

Nilsson (1996) showed that the Arctic MBL height grows with the fetch over the ice, which could introduce a false trend in the observed concentrations. To test this we have translated c_{DMS} to mass m_{DMS} per area unit by multiplying with the MBL scale height z_{box}. The resulting fit is less significant due to the smaller number of data points (only samples near the launch of a rawinsonde, see Table 1), but suggests that the slope was not significantly biased by trends in MBL depth. This should apply also to the other sulfur compounds in this study.

4.1.2. Gas-phase sulfur dioxide. In the case of SO_2(g) (Fig. 3b) both sinks and sources will influence dc_{SO_2}/dt_m. For $t_m \leqslant 3$ d the concentration decreases rapidly, so that the sinks must have been greater than the sources. For $t_m > 3$ d of transport the few values are scattered without any trend, indicating that sinks and sources on average balanced each other. The best log-linear fit slope for $t_m \leqslant 3$ d (Fig. 3b) is $k_{SO_2} = 1.1 \times 10^{-5}\,s^{-1}$, which gives an upper limit for $\tau_{0\text{-}SO_2}$ of 24 h, the turnover time had there been no source of SO_2(g). For $t_m > 3$ d we will assume a steady state between sources and sinks, since there were no significant trend in SO_2(g) with t_m.

4.1.3. Sub-micrometre aerosol MSA and nss-SO_4^{2-}. As for SO_2(g), the concentrations of MSA and nss-SO_4^{2-} decrease fast for $t_m \leqslant 3$ d (Figs. 3c and 3d), such that the sinks must have been stronger than the sources. The respective best log-linear fit slopes for $t_m \leqslant 3$ d are $k_{MSA} = 1.3 \times 10^{-5}\,s^{-1}$ and $k_{nss\text{-}SO_4^{2-}} = 1.4 \times 10^{-5}\,s^{-1}$. This corresponds to an upper limit for τ_{MSA} and $\tau_{nss\text{-}SO_4^{2-}}$ of 22 and 20 h, respectively. The similar results for both MSA and nss-SO_4^{2-} indicate that they are deposited together with the same processes, which justifies approximation (8d). There were no significant trends in MSA or nss-SO_4^{2-} after $t_m = 3$ d, so we will assume steady-state conditions for $t_m > 3$ d. There were enough aerosol samples during Julian day 229–243 to select a sub-set representing summer conditions with $k_{MSA} = 1.3 \times 10^{-5}\,s^{-1}$ and $k_{nss\text{-}SO_4^{2-}} = 1.5 \times 10^{-5}\,s^{-1}$ (Table 1). As these values are not significantly different from the overall fit, we conclude that the overall seasonal fit also is representative of the summer conditions.

4.2. Empirically estimated deposition rates

When we solve the set of equations (3) the choices of source terms Q (representing e.g. entrainment) and β will influence the results. The upper limits for the turnover times established above will serve as a guidance when choosing realistic ranges of Q and β. We will now proceed to examine if further guidance can be given by the meteorological observations and from the literature. Then we will proceed to solve the set of equations (3) and to examine what ranges of Q and β that are reasonable.

The transition from a warm and humid to a colder air mass, as marine air is transported from south of the ice edge in over the pack ice, will cause changes in most of the meteorological parameters (Serreze et al., 1995; Nilsson, 1996; Nilsson

and Bigg, 1996). Table 2 gives a summary of these changes for the IAOE-91, which will help us make a best estimate of possible deposition rates applicable for the ice covered central Arctic Ocean during summer and early autumn. There is a general lack of reported dry deposition values over pack ice, except those recently reported by Nilsson and Rannik (2001), but these where for aerosol sizes below the accumulation mode, where very little mass will be found compared to the accumulation mode. For the autumn/winter period, the surface of the multi-year pack ice is partly snow covered, and when it is bare from snow the surface is more like that of aged snow than that of sea or lake ice at lower latitudes. This will improve the number of available references on deposition rates in the literature. In Table 3 we have listed a selection of dry deposition rates for SO_2(g) and for sub-micrometre aerosol particles to ice/snow and water from the literature. For details on references in the below discussion we refer to Table 3.

4.2.1. Sub-micrometre sulfur aerosol. Dry deposition velocity for sub-micrometre particulates ($v_{\text{dry-sub-}\mu\text{m}}$) to snow should be <0.1 cm s^{-1}, particularly at stable stratified conditions (Table 3). Deposition to the water surface of leads and melt ponds should be ~ 0.5 cm s^{-1}, with smaller values at stable conditions. Combining Tables 2 and 3, it appears that an area-weighted average $v_{\text{dep-sub-}\mu\text{m}}$ should fall within 0.06–0.1 cm s^{-1}. The corresponding $\tau_{\text{dry sub-}\mu\text{m}}$ over the pack ice was estimated be around 200 h or more and $k_{\text{dry sub-}\mu\text{m}}$ on the order of 10^{-6} s^{-1}.

During the IAOE-91, the frequency of rain (f_r) and snow (f_s) was very low (Table 2). Scavenging by rain and snow is unlikely to have been important. Fogs, on the contrary, were frequent. Bergin et al. (1995a) concluded that fogs over Greenland contributed substantially to the deposition of MSA and nss-SO_4^{2-}. In our case about 35% of the aerosol mass was scavenged in fogs (Leck and Persson, 1996b). For $t_m \leqslant 3$ d advection fogs were the most persistent and had the highest drop number concentrations (N_d). The frequent radiation and mixing fogs for $t_m > 3$ d had much less duration and lower N_d, which makes them less likely to cause considerable wet deposition.

There were two drop size modes present in the fogs: always at about 25 μm in diameter and occasionally as drizzle around 100 μm (Nilsson and Bigg, 1996). This corresponds to settling velocities (V_{TS}) of about 2 and 30 cm s^{-1} for the two drop modes. Assuming that the mass ratio quoted above represents all scavenged particles, we can estimate the scavenging rate of fogs

$$\Lambda_f \approx 0.35 \frac{V_{TS}}{z_{box}} \tag{11}$$

to be on the order of $(1\text{–}2) \times 10^{-5}$ s^{-1} and $(2\text{–}3) \times 10^{-4}$ s^{-1} for the small and large drop

Table 2. *Mean values for some meteorological key parameters and their change with marine transport time*

Marine transport time (t_m), d	<0	0–1	1–2	2–3	3–4	4–5	>5
box height z_{box}, m[a)]	556	330	547	662		638	
air temperature at 30 m, °C	4.6	−0.8	−1.8	−4.0	−5.9	−5.4	−10.0
water temperature at 3 m depth, °C	6.1	−1.5	−1.6	−1.6	−1.7	−1.6	−1.6
ice temperature at 5 cm depth T_{ice}, °C	—	−0.5	−0.4	−2.6	−4.1	−5.5	
ice cover N_i[b)]	0	0.85	0.95	0.95	0.95	1.0	
total fog frequency f_f[c)]	—	0.37	0.19	0.18	0.32	0.10	—
advection fog frequency f_f[c)]	—	0.41	0.16	0.17	—	—	—
drop number concentration N_d, cm^{-3} [c)]	—	maximum 10				minimum 0.3	
				average 3.0			
total cloud cover N_c, octas	5.7	6.7	7.4	6.8	6.2	5.9	
cloud types	—	mainly St and Sc				mainly Ac and Ci	
rain frequency f_r	0.04	0.00	0.01	0.00	0.00	0.00	
dense snow fall frequency f_s	0.00	0.00	0.01	0.03	0.00	0.01	

[a)] Nilsson (1996).
[b)] Leck and Persson (1996a).
[c)] Nilsson and Bigg (1996).

Table 3. *Dry deposition of sub-micrometre aerosol and SO_2 to snow and water in the literature*

Conditions	Dry deposition velocity, cm s^{-1}	Reference height, m	References
	Dry deposition of sub-mircrometre aerosol		
snow, stable stratification	0.039	0.10	Ibrahim et al. (1983)[a)]
snow, unstable stratification	0.096	0.10	Ibrahim et al. (1983)[a)]
snow	0.023–0.062	not given	Bergin et al. (1995a)[b)]
smooth pack ice	0.03	10	Nilsson and Rannik (2001)[c)]
rough pack ice	0.04	10	Nilsson and Rannik (2001)[c)]
leads in pack ice	0.03	10	Nilsson and Rannik (2001)[c)]
water, average	0.5	5	Dolske and Sievering (1979)[d)]
water, stable stratification	0.2	5	Dolske and Sievering (1979)[d)]
	Dry deposition of SO_2		
snow, unstable stratification	1.6	2	Whelpdale and Shaw (1974)[e)]
snow, neutral stratification	0.52	2	Whelpdale and Shaw (1974)[e)]
snow, stable stratification	0.05	2	Whelpdale and Shaw (1974)[e)]
wet snow warmer than $-3\,^{\circ}C$	>0.1	not given	Granat and Johansson (1983)[f)]
	0.15	not given	Cadle et al. (1985)[g)]
dry snow colder than $-3\,^{\circ}C$	<0.1	not given	Granat and Johansson (1983)[f)]
	0.057	not given	Cadle et al. (1985)[g)]
water, neutral stratification	0.5	0.2	Owers and Powell (1974)[h)]

[a)] Ammonium sulfate particles tagged with the radioisotope ^{35}S.
[b)] Aerodynamic surrogate surfaces (airfoils).
[c)] Eddy-covariance method measuring number flux, which should be dominated by particles smaller than the accumulation mode.
[d)] Diabatic drag coefficient over water.
[e)] Gradient method.
[f)] Chamber experiment. Air was stirred in chamber, so the deposition velocity should correspond to surface resistance only with very little aerodynamic resistance, corresponding to a very small reference height.
[g)] Weekly snow samples.
[h)] $S^{35}O_2$ field experiment with an artificial lake of seawater.

modes, respectively. The latter is consistent with values for drizzle rain (Schumann, 1989).

The overall τ_{wet} due to fog deposition or drizzle can be expressed as

$$\tau_{\text{wet sub-}\mu\text{m}} \approx T_c(1-f) + \frac{1}{f\Lambda_f} \qquad (12)$$

(Rodhe and Grandell, 1972), where f is the frequency of precipitation, and T_c is the average length of the fog-free periods, which was about 12 h. For the 100 μm mode f would be the frequency of occurrence of the drizzle, about one fifth of the fog frequency f_f and the 25 μm mode. This result in a $\tau_{\text{wet sub-}\mu\text{m}}$ of about 12 h for day 1 and about 40 h for days 2–3, with the largest contribution from drizzle drops. Compared with the upper limits for τ_{MSA} and $\tau_{\text{nss-}SO_4^{2-}}$ of 22 and 20 h, it appears that fog and drizzle drop deposition can account for the entire deposition rate during day 1 and about half the deposition rate on days 2–3. It follows from eq. (12) that if the scavenging is very efficient, $\tau_{\text{wet sub-}\mu\text{m}}$ is equal to $T_c(1-f)$, which gives a lower limit of 7–10 h. We will assume $\tau_{\text{dep-sub-}\mu\text{m}}$ to be in the range 7–22 h for $t_m \leqslant 3$ and about 100–300 h for $t_m > 3$, where wet deposition by drizzle from advection fogs initially dominates over dry deposition.

4.2.2. Sulfur dioxide. SO_2(g) dry deposition velocities >0.1 cm s^{-1} have been reported for wet snow (warmer than $-3\,^{\circ}C$) and <0.1 cm s^{-1} for dry snow (colder than $-3\,^{\circ}C$), see Table 3. As seen in Table 2, the warm, melting and wet ice would be representative for relatively short t_m, while for long t_m the ice would be cold and dry. This suggests that $k_{\text{dep-}SO_2}$ should decrease with increasing t_m. Dry deposition of SO_2(g) to the open leads should also follow the decreasing trend

in ice cover (N_{ice}) with t_m. We estimate the area-weighted SO_2(g) dry deposition rate (combining Tables 2 and 3) to fall in the range $(1–6) \times 10^{-6}$ s^{-1}. This corresponds to $\tau_{dry\text{-}SO_2}$ on the order of 40–50 h for $t_m \leqslant 3$, or at least half the SO_2(g) sink during days 1–3. That would make the fog deposition over the pack ice of similar strength as that reported by Bergin et al. (1995b) to the surface on Greenland.

Oxidation of SO_2(g) to nss-SO_4^{2-} in the liquid phase by reaction with H_2O_2 (at pH < 7) (Chameides and Stelson, 1992) will contribute to $k_{SO_2 \rightarrow nss\text{-}SO_4^{2-}}$ by those drops that deposit on the surface and to $k_{SO_2 \rightarrow nss\text{-}SO_4^{2-}}$ through non-precipitating drops. From the trends in fog frequency and density (Table 2), the contribution to $k_{dep\text{-}SO_2}$ by liquid phase oxidation should have been larger for $t_m \leqslant 3$ d. Liquid phase oxidation in the cloud decks aloft will probably mainly contribute to $k_{SO_2 \rightarrow nss\text{-}SO_4^{2-}}$, since more of those drops will evaporate again. Like for the sub-micrometre sulfur aerosol, it is reasonable to assume that 7–10 h is a lower limit of $\tau_{wet\text{-}SO_2}$. In summary, $\tau_{dep\text{-}SO_2}$ is estimated to be 7–24 h and 100–300 h for $t_m \leqslant 3$ and $t_m > 3$ d, respectively.

The removal mechanism of SO_2(g) by heterogeneous loss (up to 30%) to deliquescent sea-salt particles by oxidation with O_3 (pH > 7) (Chameides and Stelson, 1992), should be insignificant considering that Leck and Persson (1996b) found only a small sub-micrometre sea-salt mass over the pack ice, compared to the open ocean.

4.3. Results from the solved system of equations

The system of eqs. (1a)–(1d) was solved with help of the approximations (8a)–(8d) for $t_m = 36$ and 96 h, in the middle of the two deposition regimes, respectively. For DMS(g) at $t_m = 36$ h we estimated all rates of change according to eqs. (2)–(4) and (6) and similarly at $t_m = 96$ h. For $t_m = 96$ h SO_2(g), MSA and nss-SO_4^{2-} were assumed to be in steady state. Inserted into eq. (1) these estimates will feed information into the system of equations about the speed with which the sulfur compounds were formed, destroyed and removed.

4.3.1. Deposition rates and deduced values of β. For $t_m = 96$ h and $\beta = 0$ both $k_{dep\text{-}sub\text{-}\mu m}$ and $k_{SO_2 \rightarrow nss\text{-}SO_4^{2-}} + k_{dep\text{-}SO_2}$ are much larger than our earlier estimated upper range. Relatively high c_{DMS} and the large k_{DMS} cause these unrealistic deposition rates. This would require SO_2(g), nss-SO_4^{2-} and MSA to be destroyed very fast to compensate for the production. For $t_m = 96$ h, the previously established limits of $\tau_{dep\text{-}sub\text{-}\mu m}$ and $\tau_{0\text{-}SO_2}$ correspond to a range of $1.8 < \beta < 6.9$. The $t_m = 96$ h solutions have slightly negative $k_{dep\text{-}SO_2}$ for any β, which we will deal with in the next section. The deposition rates of SO_2(g) and of the sulfur aerosol are much higher in the 36 h case, compared to the 96 h. For $\beta > 6.4$ $k_{SO_2 \rightarrow nss\text{-}SO_4^{2-}}$ is negative.

In summary, this suggests a range of $1.8 < \beta < 6.4$, which implies that between 64 and 86% of the DMS(g) was not converted to SO_2(g) and sulfur aerosol. Similar results have been found in remote regions elsewhere by Huebert et al. (1993; 1996), who suggested that >50 and 66% of the DMS(g), respectively, was not converted to SO_2(g) and sulfur aerosol. Probably DMS(g) was instead converted into DMSO or $DMSO_2$ (Hynes et al., 1996; Berrescheim et al., 1993). In the remaining calculations we will use $\beta = 3$, corresponding to 75%, in the middle of the range established above.

4.3.2. Sources and sinks due to entrainment/detrainment. Considering the MBL evolution and high stability over the pack we have probably no significant exchange between the FT and the MBL for small t_m. With increasing t_m the MBL will be less stable, but deeper, with some entrainment. In most cases one would expect higher SO_2(g) and nss-SO_4^{2-} concentrations in the FT than in the MBL (Ferek et al., 1995), so the net fluxes should be downward.

For any β at $t_m = 96$ h we find negative $k_{dep\text{-}SO_2}$ caused by the large oxidation rate of SO_2(g) compared to production rate, unless we introduce an external source of SO_2(g) or nss-SO_4^{2-}. Based on similar arguments as used to establish the range of β, we find that $Q_{nss\text{-}SO_4^{2-}}$ must be within the range of $(0.1–6.1) \times 10^{-7}$ nmol m^{-3} s^{-1} for $t_m = 96$ h. This is on the same order of magnitude as the nss-SO_4^{2-} production and sink. For $t_m = 36$ h $Q_{nss\text{-}SO_4^{2-}}$ has to be $< 4 \times 10^{-7}$ nmol m^{-3} s^{-1} to avoid negative $k_{SO_2 \rightarrow nss\text{-}SO_4^{2-}}$, and Q_{SO_2} has to be $> 8 \times 10^{-12}$ nmol m^{-3} s^{-1}, a negligible contribution, which indicates that nss-SO_4^{2-} is a more substantial FT sulfur source than SO_2(g).

Detrainment could also be a DMS(g) sink, but it turns out that such a sink has only marginal influences on the resulting sink rates and is not necessary to explain our observations.

4.3.3. Estimation of uncertainty. For DMS(g), the 95% confidence interval of the fit in Fig. 3a is probably the best measure of the uncertainty and the large natural variability in the seasonal average. At $t_m = 36$ h, the 95% confidence interval of the slope of the fits to SO_2, MSA and nss-SO_4^{2-} from Table 1 propagate through the system of equations (3). If we combine the standard deviations with the full range of values that we consider realistic for β and $Q_{\text{nss-SO}_4^{2-}}$, an estimate of the overall uncertainty of the turnover times can be made (Table 4). They agree well with the previously estimated upper and lower limits for the turnover times. For the $t_m = 96$ h case these ranges of uncertainty are comparable to our previous estimates of 100–300 h.

We have tested other combinations of approximations than (8a)–(8d), but found these to give impossible or less likely results than the ones that were chosen. If we for example exclude approximation (8b) and allow a reaction path from DMS(g) directly to nss-SO_4^{2-} and/or assume that $k_{\text{DMS}\rightarrow ?} = 0$, we arrive at very peculiar results, including backward sink and oxidation, which we can only compensate for with very large unrealistic DMS flux from the FT. If approximation (8a) and/or (8d) are not used, we also get unrealistic results, but they confirm that α is close to 0.22 for our data set.

5. Concluding discussion

We have derived several quantitative and qualitative results related to the sulfur budget in the remote Arctic MBL summer and autumn, summarized in Table 4. Figure 4 shows the sulfur budget obtained from the solutions of the system of equations (3) with $\beta = 3$ and $Q_{\text{nss-SO}_4^{2-}} = 0$ at $t_m = 36 \times 10^{-7}$ and 3×10^{-7} nmol m^{-3} s^{-1} at $t_m = 96$ h. Other choices of α, β, Q and S terms would give somewhat different solutions. However, the fluxes in Fig. 4 are internally consistent and represent our best understanding of the sulfur budget during IAOE-91. Imbedded in the pseudo-Lagrangian approach follows that these conclusions apply to periods with advection of

Table 4. *Summary of results for the atmospheric sulfur budget in the Arctic remote marine boundary layer*

	Best estimate	Range of uncertainty	Literature comparison
		DMS(g) for all t_m	
$\tau_{0\text{-DMS}}$	59 h	53–76 h	from 13 h[a] to 7–9 days[b]
β	3 (75%)	1.8–6.4 (64–86%)	>50%[b], 66%[c]
		SO_2(g), MSA and nss-SO_4^{2-} for $t_m = 36$ h (days 1–3)	
$\tau_{0\text{-SO}_2}$	16 h	10–24 h	15 ± 3 h[d], 8–24 h[b]
$\tau_{0\text{-MSA}}$	18 h	15–22 h	31 h, same as for nss-SO_4^{2-} [a]
$\tau_{0\text{-SO}_4^{2-}}$	18 h	15–20 h	from 1 day[e] to 2 days[f]
		SO_2(g), MSA and nss-SO_4^{2-} for $t_m = 96$ h (days 4–5)	
$\tau_{0\text{-SO}_2}$	173 h	100–300 h	
$\tau_{0\text{-MSA}}$	186 h	100–300 h	100 h[g]
$\tau_{0\text{-SO}_4^{2-}}$	186 h	100–300 h	100 h[g]
$Q_{\text{nss-SO}_4^{2-}}$ from FT	3×10^{-7} nmol m^{-3} s^{-1}	$(0.1\text{–}6.1) \times 10^{-7}$ nmol m^{-3} s^{-1}	
Q_{SO_2} from FT	—	$> 8 \times 10^{-12}$ nmol m^{-3} s^{-1}	

[a] Bates et al. (1990).
[b] Davis et al. (1998).
[c] Huebert et al. (1996).
[d] Bonsang et al. (1987).
[e] Huebert et al. (1990).
[f] Vong et al. (1988).
[g] Nilsson and Rannik (2001); applies to aerosol particles of sizes below the accumulation mode. For accumulation mode mass this should be regarded as a lower limit.

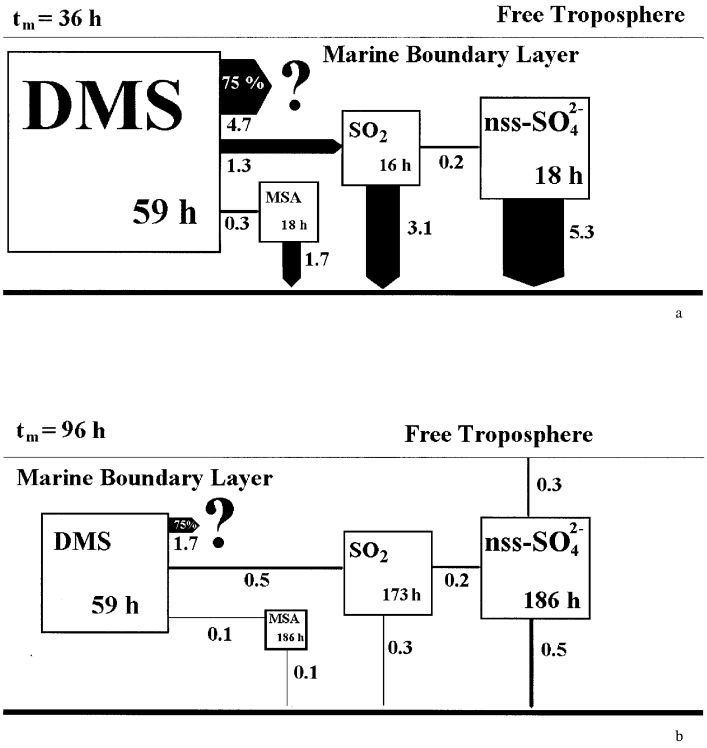

Fig. 4. (a) Budget for the atmospheric part of the natural sulfur cycle in the remote Arctic marine boundary layer in summer of 1991, for $t_m = 36$ h, $\beta = 3$, and $Q_{\text{nss-SO}_4^{2-}} = 0$. The concentration of each sulfur compound is proportional to the area of each box, where the DMS box, for example, represents 1.34 nmol m^{-3}. The widths of the arrows represent the fluxes given in units of 10^{-6} nmol m^{-3} s^{-1}. The times given in the boxes are the turnover times in hours. (b) Same as (a), but for $t_m = 96$ h with $Q_{\text{nss-SO}_4^{2-}} = 3 \times 10^{-7}$ nmol m^{-3} s^{-1}.

marine air into the central Arctic Ocean. It may be that our conclusions are mainly representative for the European sector of the central Arctic Ocean, where on average the most frequent import of marine air can be expected (Serreze et al., 1995).

The DMS(g) turnover time has been estimated as $\sim$59 h, which agrees well with those of Huebert et al. (1993) and Chen et al. (1999) of 3 d and $\leqslant$2.5 d, respectively. The lack of seasonal difference in $\tau_{0\text{-DMS}}$ indicates that an increase in the NO_3 radical concentration compensated for the decrease in OH radical concentration as the dark season approached. In agreement with Huebert et al. (1993; 1996) we concluded that a large fraction ($\sim$75%) of the DMS(g) does not form SO_2(g), MSA or nss-SO_4^{2-}, at least not in this study region. A direct oxidation of DMS(g) to nss-SO_4^{2-} via the SO_3 is indicated to be less important than the oxidation from SO_2(g).

In marine air aged up to 3 d over the ice-covered central Arctic Ocean we found wet deposition by drizzle and fog drops to be the dominant sink of sub-micrometre sulfur aerosol. This corresponds to a turnover time of 15–22 h, which is slightly smaller than found by Bates et al. (1990) and Vong et al. (1988), who reported values between 1 and 2 d. Beyond 3 d of transport only less efficient deposition processes remain, as a result of less drizzle and less dense fogs, corresponding to turnover times of several days.

The same applies to SO_2, for which we found the turnover time to be 10–24 h, in excellent agreement with Bonsang et al. (1987) and Davis et al. (1998), who reported 12–18 and 10–24 h, respectively. Aqueous phase oxidation in fog drops prior to their precipitation and dry deposition to open leads and wet and warm ice floes must have been important. Beyond 3 d $\tau_{0\text{-SO}_2}$ the increased

to several days, owing to lower fog density and duration, the increase in ice cover and the change to frozen and dry ice surface. For air aged >3 d over the pack ice a net flux from the FT of nss-SO_4^{2-} is necessary.

5.1. Relations between turnover times and timescales of transport

If we compare the turnover times we have derived with the frequency distribution of t_m in Fig. 5, we can make some reflections. Firstly, although DMS lacks a significant source over most of the pack ice (Leck and Persson, 1996a), it will be advected far in over the pack ice from the surrounding open seas during cyclone activity and on ice air flow. Secondly, as wet deposition of the sub-micrometre sulfur aerosol and SO_2 is so large during on ice air flow, much of the aerosol sulfur mass that entered the pack ice area will be scavenged during the first day over the pack ice.

Combined, this selective 'filter' effect suggests that much of the MBL sub-micrometre sulfur aerosol over the central Arctic Ocean originates from *in-situ* aerosol formation and growth from DMS oxidation products, with a contribution, perhaps of equal magnitude, from the FT. Thus the large DMS sources south of the ice edge and its advection in over the pack ice are more important for the evolution and the properties of sub-micrometre sulfur aerosol than the advection of aerosols into the central Arctic Ocean. The DMS(g) turnover time of 59 h is on the same order of magnitude as the median t_m of 55 h. Therefore changes in transport patterns from one day to another, from one season to another or from one year to another should have large effects on the atmospheric sulfur budget of the central Arctic Ocean. Indeed, when a similar scientific program was conducted on the Arctic Ocean Expedition in 1996, in approximately the same season and sector, the median t_m was >120 h. The difference was mainly caused by less cyclone activity and intensity during the 1996 expedition (Maslinik et al., 1996; Nilsson and Barr, 2001). This caused air masses to reside over the pack ice for periods of 10 d or more in anti-cyclonic circulations, and brought much less marine air in over the pack ice. In such conditions, the sulfur budget in Fig. 4b may still be valid, but it is also possible that entrainment and large-scale subsidence played a more important role.

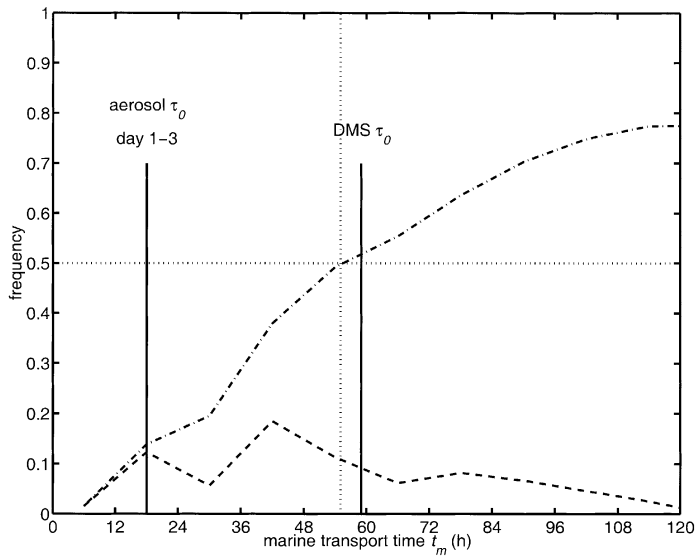

Fig. 5. The frequency (dashed line) distribution of marine transport times during the IAOE-91, the cumulative frequency (dashed dotted line), and the 50% median (dotted lines). The turnover time for DMS(g) and the turnover time for the sub-micrometre sulfur aerosol during days 1–3 over the pack ice are also indicated.

5.2. *Possibilities for climate effects in the central Arctic Ocean of DMS seawater production*

Curry (1995) argues that it is unlikely that there would be a substantial climatic DMS feed-back over the central Arctic Ocean, partly because of the limited DMS sources within the pack ice. However, atmospheric transport will provide the air over the pack ice with DMS (Leck and Persson, 1996b). The selective 'filter' effect (Fig. 5) will enforce a possible climate effect of DMS production over the central Arctic Ocean, through *in-situ* formed CCN. Since the warm air advection from south contributes much to the ice melting during summer, changes in cloud and fog albedo in this air due to changes in CCN concentration following changes in DMS emissions could have relevant climate effects.

For the central Arctic Ocean the original phytoplankton–DMS–climate feedback hypothesis, as proposed by Charlson et al. (1987), can hardly apply for very simple reasons. The potential climate effect of DMS production over the pack ice covered central Arctic Ocean is down-wind of the DMS source and cannot locally feed back to the source. Furthermore, changes in the surface energy budget following upon changes in cloud and fog albedo may change the ice melting, but will not impact much on air and water temperature.

On the other hand, DMS emissions could feed back negatively owing to changes in the productive areas caused by changes in the pack ice extent. A decreased ice cover would change the present overall production of DMS and biogenic CCN in the region considerably from that calculated by Leck and Persson (1996a). Therefore, we can suggest a modification of the hypothesis of Charlson et al. (1987), an ice–DMS–cloud–albedo feedback responding to a negative feedback upon changes in pack ice extent.

However, recent observations indicate a 7% per decade decrease in perennial multi-year ice extent (Johannessen et al., 1999), a 0.1 m per year decrease in average ice thickness (Rothrock et al., 1999) and a 2.6 d per decade increase in melt season (Rigor et al., 2000) in the Arctic Ocean. This may be the first signs of a rapidly declining central Arctic pack ice, owing to increased greenhouse warming and related positive feedback effects. These observations suggest that the ice–DMS–cloud–albedo feedback is less significant than other (positive) ice feedback mechanisms, such as the ice–albedo and ice–heat–flux feedbacks. It may, however, still be necessary to understand the ice–DMS–cloud–albedo feedback to achieve a complete understanding of the climate mechanisms of the high Arctic.

5.3. *Possible effects of increased anthropogenic aerosols in the central Arctic Ocean*

As long as the cloud and fog life times and precipitation rates are not considerably changed by the aerosol, the system may be less sensitive to moderate increases in antrophogenic aerosols in the summer than in other seasons thanks to the selective 'filter' effect. Increased number of anthropogenic CCNs, either due to changed atmospheric transport patterns or due to increased anthropogenic emissions within the Arctic, may change the drop spectra and lifetime of the clouds and fogs enough to considerably decrease the 'filter' effect. However, changes in transport pattern would also change heat and moisture advection, such that pollutants would be injected into the Arctic with heat and moisture, which may have larger effects than the aerosol on clouds and fog. Increased anthropogenic emissions of sulfur aerosols within the Arctic could both increase cloud/fog albedo and extent. This could influence the air mass transformation and the summer ice melting.

6. Acknowledgements

We acknowledge K. Bigg, C. Persson and H. Rodhe for valuable criticism during the preparation of this work. We are obliged to ECMWF for the use of their database, computing facilities and for the support from their staff. We thank R. McGrath for allowing us to use his trajectory model and for his technical support with the model. This research was supported by grants from the Swedish Natural Science Research Council (contract E-EG/GU 9906-30 and E-EG 3922-313) and The Knut and Alice Wallenberg Foundation.

REFERENCES

Bandy, A. R., Scott, D. L., Blomqvist, B. W., Shen, S. M. and Thornton, D. C. 1992. Low yields of SO_2 from dimethyl sulfide oxidation in the marine boundary layer. *Geophys. Res. Lett.,* **19**, 1125–1127.

Bates, T. S., Johnson, J. S., Quinn, P. K., Goldan, P. D., Kuster, W. C., Covert, D. C. and Hahn, C. J. 1990. The biogeochemical sulfur cycle in the marine boundary layer over the northeast pacific ocean. *J. Atmos. Chem.* **11**, 59–81.

Bergin, M. H., Jaffrezo, J. L., Davidson, C. I., Dibb, J. E., Pandis, S. N., Hillamo, R., Maenhaut, W., Kuhns, H. D. and Mäkelä, T. 1995a. The contribution of snow, fog, and dry deposition to the summer flux of anions and cations at Summit, Greenland. *J. Geophys. Res.* **100**, 16,275–16,288.

Bergin, M. H., Pandis, S. N., Davidson, C. I., Jaffrezo, J.-L., Dibb, J. E., Russel, A. G. and Kuhns, H. D. 1995b. Modeling of the processing and removal of trace gas and aerosol species by Arctic radiation fogs and comparison with measurements. *J. Geophys. Res.* **101**, 14,465–14,478.

Berrescheim, H., Eisle, F. L., Tanner, D. J., McInnes, L. M., Ramsey-Bell, D. C. and Covert, D. S. 1993. Atmospheric sulfur chemistry and cloud condensation nuclei (CCN) concentrations over the northeastern pacific coast. *J. Geophys. Res.* **98**, 12,701–12,711.

Bigg, E. K. 1996. Ion induced nucleation around radon daughters in remote Arctic maritime air. *Tellus* **48B**, 322–328.

Bonsang, B., Nguyen, B. C. and Lambert, G. 1987. Comment on 'the residence time of aerosols and SO_2 in the long range transport over the ocean', by Ito et al. *J. Atmos. Chem.* **5**, 367–369.

Caddle, S. H., Dash, J. M. and Mulawa, P. A. 1985. Atmospheric concentrations and the deposition velocity to snow of nitric acid, sulphur dioxide, and various particulate species. *Atmos. Environ.* **19**, 1819–1827.

Campolongo, F., Saltelli, A., Jensen, N. R., Wilson, J. and Hjorth, J. 1999. The role of multiphase chemistry in the oxidation of dimethylsulphide (DMS). A latitude dependent analysis. *J. Atmos. Chem.* **32**, 327–356.

Capaldo, K. P. and Pandis, S. N. 1997. Dimethylsulfide chemistry in the remote marine atmosphere: evaluation and sensitivity analysis of available mechanisms. *J. Geophys. Res.* **102**, D19, 23,251–23,267.

Chameides, W. L. and Stelson, A. W. 1992. Aqueous-phase chemical processes in deliquescent sea-salt aerosols: a mechanism that couples the atmospheric cycles of S and sea salt. *J. Geophys. Res.* **97**, D18, 20,565–20,580.

Charlson, R. J., Lovelock, J. E., Andreae, M. O. and Warren, S. G. 1987. Oceanic phytoplankton, atmospheric sulphur, cloud albedo and climate. *Nature* **326**, 655–661.

Chen, G., Davis, D., Kasibhatla, P., Bandy, P., Bandy, A., Thornton, D. and Blake, D. 1999. A mass-balance/photochemical assessment of DMS sea-to-air flux as inferred from NASA GTE PEM-West A and B observations. *J. Geophys. Res.* **104**, D5, 5471–5482.

Curry, J. A. 1995. Interactions among aerosols, clouds, and climate of the Arctic Ocean. *Sci. of Total Environ.* **160/161**, 777–791.

Dolske, D. A. and Sievering, H. 1979. Trace element loading of southern lake Michigan by dry deposition of atmospheric aerosols. *Water Air Soil Pollut.* **12**, 485–502.

Davis, D., Chen, G., Kasibhatle, P., Jefferson, A., Tanner, D., Eisele, F., Lenshow, D., Neff, W. and Berresheim, H. 1998. DMS oxidation in the Antarctic marine boundary layer: comparasion of model simulations and field observations of DMS, DMSO, $DMSO_2$, H_2SO_4(g), MSA(g) and MSA(p). *J. Geophys. Res.* **103**, D1, 1657–1678.

Ferek, R. J., Hobbs, P. V., Radke, L. F., Herring, J. A., Sturges, W. T. and Cota, G. F. 1995. Dimethyl sulfide in the arctic atmosphere. *J. Geophys. Res.* **100**, D12, 26,093–26,104.

Granat L. and Johansson, C. 1983. Dry deposition of SO_2 and NO_x in winter. *Atmos. Environ.* **17**, 191–192.

Huebert, B. J., Howell, S., Laj, P., Johnson, J., Bates, T. S., Quinn, P. K., Yegorov, V., Clarke, A. D. and Porter, J. N. 1993. Observations of the atmospheric sulfur cycle on SAGA 3. *J. Geophys. Res.* **98**, D9, 16,985–16,995.

Huebert, B. J., Wylie, D. J., Zhuang, L. and Heath, J. A. 1996. Production and loss of methanesulfonate and non-sea salt sulfate in the equatorial Pacific marine boundary layer. *Geoph. Res. Lett.* **23**, 737–740.

Hynes, A. J. and Wine, P. H. 1996. The atmospheric chemistry of dimethylsulfoxide (DMSO) and mechanism of the OH + DMSO reaction, *J. Atmos. Chem.* **24**, 23–37.

Ibrahim, M., Barrie, L. A. and Fanaki, F. 1983. An experimental and theoretical investigation of the dry deposition of particles to snow, pine trees and artificial collectors. *Atmos. Environ.* **4**, 781–788.

Johannessen, O. M, Shalina, E. V. and Miles, M. W. 1999. Satellite evidence for an Arctic sea ice cover in transformation. *Science* **286**, 1937–1939.

Johnson, D. W., Osborne, S., Wood, R., Suhre, K., Johnson, R., Bussinger, S., Quinn, R. K., Wiedensohler, A., Durkee, P. A., Russel, L. M., Andreae, M. O., O'Dowd, C., Noone, K. J., Bandy, B., Rudolph, J. and Rapsomanikis, S. 2000. An overview of the Lagrangian experiment undertaken during the North Atlantic regional Aerosol Characterisation Experiment (ACE-2). *Tellus* **52B**, 290–320.

Koga, S. and Tanaka, H. 1999. Modeling the methanesulfonate to non-sea-salt sulfate molar ratio and dimethylsulfide oxidation in the atmosphere. *J. Geophys. Res.* **104**, D11, 13,735–13,747.

Leck, C. and Persson, C. 1996a. The central Arctic Ocean

as a source of dimethylsulfide. seasonal variability in relation to biological activity. *Tellus* **48B**, 156–177.

Leck, C. and Persson, C. 1996b. Seasonal and short-term variability in dimethyl sulfide, sulfur dioxide and biogenic sulfur and sea salt aerosol particles in the marine boundary layer during summer and autumn. *Tellus* **48B**, 272–299.

Leck, C., Bigg, E. K., Covert, D. S., Heintzenberg, J., Maenhaut, W., Nilsson, E. D. and Wiedensohler, A. 1996. Overview of the atmospheric research program during the International Arctic Ocean Expedition 1991 and its scientific results. *Tellus* **48B**, 136–155.

Lee, Y.-N. and Zhou, K. 1994. Aqueous reaction kinetics of ozone and dimethylsulfide and its atmospheric implications. *J. Geophys. Res.* **99**, D2, 3597–3605.

Liljeström, G. (ed.) 1992. *Icebreaker Oden trafficability data — International Arctic Ocean Expedition 1991*. Swedish Arctic Research Programme, Swedish Polar Research Secretary, Box 50005, S-104 05 Stockholm, Sweden.

Lin, X. and Chamides, W. L. 1993. CCN formation from DMS oxidation without SO_2 acting as an intermediate. *J. Geophys. Res.* **20**, 579–582.

Maslanik, J. A., Serreze, M. C. and Barry, R. G. 1996. Recent decreases in Arctic summer ice cover and linkages to atmospheric ciculation anomalies. *Geophys. Res. Lett.* **23**, 1677–1680.

McGrath, R. 1989. Trajectory models and their use in the Irish Meteorological Service. memorandum no. 112/89, Irish Meteorological Service, Dublin.

Nilsson, E. D. 1996. Planetary boundary layer structure, transport and weather during the International Arctic Ocean Expedition 1991. *Tellus* **48B**, 178–196.

Nilsson, E. D. and Barr, S. 2001. Effects of synoptic patterns on atmospheric chemistry and aerosols during the Arctic Ocean Expedition 1996. *J. Geophys. Res.*, **106**, 32,609–32,086.

Nilsson, E. D. and Bigg, E. K. 1996. Influences on formation and dissipation of high arctic fogs during summer and autumn and their interaction with aerosol. *Tellus* **48B**, 234–253.

Nilsson, E. D. and Rannik, Ü. 2001. Turbulent aerosol fluxes over the Arctic Ocean 1. Dry deposition over sea and pack ice. *J. Geophys. Res.*, **106**, 32,125–32,138.

Nilsson, E. D., Rannik, Ü and Hákansson, M. 2001. Surface energy budget over the central Arctic Ocean during late summer and early freeze-up. *J. Geophys. Res.*, **106**, 32,187–32,206.

Owers, M. J. and Powell, A. W. 1974. Deposition velocity of sulfur dioxide on land and water using a ^{35}S method. *Atmos. Environ.* **8**, 63–67.

Paluch I. R., Lenschow, D. H. and Wang, Q. 1997. Arctic boundary layer in the fall season over open and frozen sea. *J. Geophys. Res.* **102**, D22, 25,955–25,971.

Persson, C. and Leck, C., 1994. Determination of reduced sulfur compounds in the atmosphere using a cotton scrubber for oxidation removal and gas chromatography with flame photometric detection. *Anal. Chem.* **66**, 983–987.

Rigor, I. G., Colony, R. L. and Martin, S. 2000. Variations in surface air temperature observations in the Arctic. 1979–97. *J. Climate* **13**, 896–914.

Rodhe, H. and Grandell, J. 1972. On the removal time of aerosol particles from the atmosphere by precipitation scavenging. *Tellus* **24**, 442–454.

Rothrock, D. A., Yu, Y. and Maykut, G. A. 1999. Thinning of the Arctic sea ice cover. *Geophys. Res. Lett.* **26**, 3469–3472.

Schumann, T. 1989. Large discrepancies between theoretical and field-determined scavenging coefficients. *J. Aerosol Sci.* **20**, 1159–1162.

Serreze, M. C., Rehder, M. C., Barry, R. G., Kahl, J. D. and Zaitseva, N. A. 1995. The distribution and transport of atmospheric water vapor over the Arctic Basin. *Int. J. Climatol.* **15**, 709–727.

Stumm, W. and Morgan, J. J. 1981. *Aquatic chemistry*. Wiley, New York, 1–780.

Twomey, S. 1974. Pollution and planetary albedo. *Atmos. Environ.* **8**, 1251–1256.

Vong, R. J., Hansson, H.-C., Ross, H. B., Covert, D. S. and Charlson, R. J. 1988. Northeast Pacific submicrometer aerosol and rainwater composition. *J. Geophys. Res.* **93**, 1625–1637.

Whelpdale, D. M. and Shaw, R. W. 1974. Sulfur dioxide removal by turbulent transfer over gases, snow and other surfaces. *Tellus* **26**, 196–204.

Yin, F., Grosjean, D. and Seinfeld, J. H. 1990a. Photooxidation of dimethylsulfide and dimethyldisulfide: mechanism development. *J. Atmos. Chem.* **11**, 309–364.

Yin, F., Grosjean, D., Flagan, R. C., and Seinfeld, J. H. 1990b. Photo-oxidation of dimethylsulfide and dimethyldisulfide: mechanism evaluation. *J. Atmos. Chem.* **11**, 365–399.